Constrained Attitude Control of Over-actuated Spacecraft Subject to Instrument Pointing Direction Deviation

Zeyu Kang, Qiang Shen and Shufan Wu

***Abstract*— In this paper, the attitude reorientation problem for over-actuated rigid spacecraft subject to multiple attitude constrained zones is studied. Considering the pointing direction deviation of sensitive equipments and constraint operating set, a robust potential function for attitude constrained zones is proposed and is further leveraged to design a high-level attitude controller, which achieves asymptotic convergence of attitude reorientation error while avoiding attitude constrained zones. Moreover, to distribute the desired control torque from high-level controller to each actuator dynamically, a finite-time adaptive control allocation is developed, resulting in an improved allocation error convergence rate when compared with existing control allocation methods. Simulation examples involving a rest-to-rest attitude maneuver are given to demonstrate the effectiveness of the proposed overall control strategy.**

***Index Terms*— Constrained control; Robust adaptive control; Lyapunov methods**

I. Introduction

SPACECRAFT attitude control is widely studied in the control community. A series of nonlinear control algorithms are proposed for attitude control, such as backstepping control [1], sliding mode control [2], adaptive control [3], inverse optimal control [4] and others. To improve the autonomy and safety, large angle reorientation under attitude constraints and actuator redundancy have attracted great interest recently.

Spacecraft is often equipped with sensitive instruments that have to avoid direct exposure to bright celestials during attitude maneuver. Approaches for solving this constrained attitude control problem can be categorized into path planning-based and potential function-based methods. Several attitude path planning strategies have been developed to find the allowable rotation trajectory [5]. However, these methods have complex structure and expensive computation. In contrast, the potential function-based method incorporates an artificial potential in attitude controller design, so that the derived analytical controller is suitable for on-board application. In [6], Lee proposed a convex logarithmic barrier potential in unit-quaternion space, which was subsequently utilized to design an attitude controller that ensures attitude convergence and satisfies constraints caused by attitude mandatory and constrained zones. In [7], the potential function was constructed as a Gaussian function for spacecraft attitude control. In [8], [9], based on the unit-quaternion parameterized attitude-constrained zones, a quadratic potential function was developed to parametrize the constrained zones. However, above mentioned potential functions do not consider pointing direction deviation of airborne equipment caused by installation misalignments, vibrations and measurement errors, which could lead to attitude constraint violation and damages to sensitive equipments.

For over-actuated systems, control allocation (CA) is widely used to manage actuator redundancy, which assigns the desired control command from the high-level virtual controller to available low-level actuators optimally [10]. In [11], [12], the adaptive high-level controllers and robust CA obtained by solving a second-order cone program were proposed for fault-tolerant attitude tracking of spacecraft. Although these CA methods work well theoretically, they require solving a constrained optimization problem statically within each sampling period, which may not be practical due to the limited on-board computation resources. To tackle this issue, the dynamic CA is developed by constructing an updating law such that the CA optimization problem converges to the optimal solution dynamically [13]. In [14], the adaptive CA was studied comprehensively. In [15], adaptive CA scheme was proposed for over-actuated vehicles. In [16], a dynamic near optimal control allocation combined with saturated baseline controller was proposed for attitude control. However, the CA convergence time is not addressed in above mentioned methods, which may lead to large allocation errors during CA convergence process.

In this paper, we proposed a finite-time adaptive CA-based attitude controller for over-actuated spacecraft subject to attitude constrained zones and pointing direction deviation of sensitive equipment. First, A warning angle-based robust potential function being leveraged for constructing a high-level attitude controller is proposed for attitude constraints. Then, a finite-time adaptive CA that distributes the desired control torque from high-level controller to each actuator is developed. The main contributions of this paper are two-fold: 1) Comparing with existing potential functions [6]–[9] for attitude constraints, the proposed warning angle-based potential function not only is robust against pointing direction deviation but also prevents from using the constrained zones far away from sensitive instruments, and hence enhances safety for

The authors are with school of Aeronautics and Astronautics, Shanghai Jiao Tong University, Shanghai, China, 200240 (email: {kangzeyu, qiangshen, shufan.wu}@sjtu.edu.cn).

This work was sponsored by Natural Science Foundation of Shanghai under grant 20ZR1427000, Shanghai Sailing Program under grant 20YF1421600, and China State Key Laboratory of Robotics under grant 19Z1240010018.

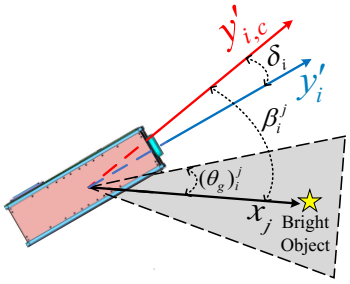

Fig. 1: Demonstration of attitude constrained zone.

sensitive equipment; 2) Different from existing dynamical CA approches in [14]–[16], the proposed approach achieves finite-time convergence of the dynamical CA, resulting in improved convergence rate and steady-state accuracy of allocation error. To our best knowledge, this is the first time that warning angle and pointing direction deviation of sensitive instrument are simultaneously considered in synthesizing potential functions for attitude constraints. Finally, we demonstrate the effectiveness of the proposed overall controller.

II. Preliminaries

A. Kinematics and Dynamics Equation

In this paper, the unit quaternion given by

$$\mathbb{Q}_u = \{\boldsymbol{Q} = \left[\boldsymbol{q}^T, q_0\right]^T \in \mathbb{R}^3 \times \mathbb{R} \mid \boldsymbol{q}^T\boldsymbol{q} + q_0^2 = 1\}, \quad (1)$$

is used to parameterize the attitude, where $\boldsymbol{q} \in \mathbb{R}^3$ and $q_0 \in \mathbb{R}$ represent vector part and scalar part of the quaternion.

The unit-quaternion conjugate or inverse is defined as $\boldsymbol{Q}^* = \left[-\boldsymbol{q}^T, q_0\right]^T$. Let $\boldsymbol{Q}_d \in \mathbb{Q}_u$ denote the desired attitude. The unit-quaternion error $\boldsymbol{Q}_e = [q_{e1}, q_{e2}, q_{e3}, q_{e0}]^T = \left[\boldsymbol{q}_e^T, q_{e0}\right]^T \in \mathbb{Q}_u$ is given by $\boldsymbol{Q}_e = \boldsymbol{Q}_d^* \otimes \boldsymbol{Q} = \left[\boldsymbol{q}_e^T, q_{e0}\right]^T$, where $\otimes$ denotes the quaternion multiplication operator. Let $\boldsymbol{\omega}_d$ denote the desired angular velocity in the desired reference frame $\mathcal{N}$. Since the rest-to-rest attitude maneuver is considered, $\boldsymbol{\omega}_d = 0$, and hence $\boldsymbol{\omega}_e = \boldsymbol{\omega}$, where $\boldsymbol{\omega} \in \mathbb{R}^3$ is the angular velocity of the spacecraft with respect to an inertial frame $\mathcal{I}$ and expressed in the body frame $\mathcal{B}$.

Then, the kinematics and dynamics of the over-actuated spacecraft with $N > 3$ actuators can be described as [11]:

$$\dot{\boldsymbol{Q}}_e = \frac{1}{2}\begin{bmatrix}\boldsymbol{S}(\boldsymbol{q}_e) + q_{e0}\boldsymbol{I}_3 \\ -\boldsymbol{q}_e^T\end{bmatrix}\boldsymbol{\omega} \quad (2)$$

$$\boldsymbol{J}\dot{\boldsymbol{\omega}}(t) = -\boldsymbol{S}(\boldsymbol{\omega})(t)\boldsymbol{J}\boldsymbol{\omega}(t) + \boldsymbol{u}(t) + \boldsymbol{d}(t), \quad (3)$$

where the matrix $\boldsymbol{S}(\boldsymbol{x}) \in \mathbb{R}^{3\times3}$ is a skew-symmetric matrix, $\boldsymbol{J} \in \mathbb{R}^{3\times3}$ is the inertia matrix of the spacecraft, the environmental disturbance is denoted as $\boldsymbol{d}(t) \in \mathbb{R}^3$, and $\boldsymbol{u}(t) \in \mathbb{R}^3$ is the total external control torque given by

$$\boldsymbol{u}(t) = \boldsymbol{D}\boldsymbol{\tau}(t), \quad (4)$$

where $\boldsymbol{D} \in \mathbb{R}^{3\times N}$ and $\boldsymbol{\tau}(t) \in \mathbb{R}^N$ are actuator configuration matrix and the output vector, respectively. Since the spacecraft is over-actuated, the condition $\text{rank}(\boldsymbol{D}) = 3$ is satisfied. For brevity, the time argument t is hereafter left out.

Assumption 1: The external disturbance $\boldsymbol{d}$ is bounded by $\|\boldsymbol{d}\| \leq \boldsymbol{d}_{\max}$, where $\boldsymbol{d}_{\max}$ is a positive constant and $\|*\|$ denotes the Euclidean norm.

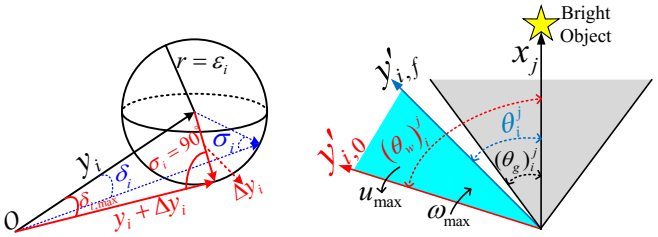

(a) Equipment pointing deviation (b) Warning zone

Fig. 2: Schematic of equipment pointing deviation and warning zone.

B. Attitude Constrained Zones

Definition 1 (Attitude Constrained Zone): The set of attitudes that airborne sensitive equipments (e.g., infrared telescopes) directly expose to certain celestial objects (e.g., the sun) is considered an attitude constrained zone. Multiple constrained zones can be specified with respect to a single airborne equipment boresight vector.

Attitude constrained zone is associated with instrument boresight vector, whose nominal and actual pointing directions are expressed in the body frame $\mathcal{B}$ as $\boldsymbol{y}_i$ and $\boldsymbol{y}_{i,c}$. The actual pointing direction vector in the inertial frame $\mathcal{I}$ is obtained by

$$\begin{aligned}\boldsymbol{y}'_{i,c} &= \boldsymbol{Q} \otimes \boldsymbol{y}_{i,c} \otimes \boldsymbol{Q}^* \\ &= \boldsymbol{y}_{i,c} - 2(\boldsymbol{q}^T\boldsymbol{q})\boldsymbol{y}_{i,c} + 2(\boldsymbol{q}^T\boldsymbol{y}_{i,c})\boldsymbol{q} + 2q_0(\boldsymbol{y}_{i,c} \times \boldsymbol{q}).\end{aligned} \quad (5)$$

As shown in Fig. 1, for the i-th sensitive equipment (e.g., an infrared telescope), to avoid the attitude-forbbidden zone, an angle β_i^j being strictly greater than $(\theta_g)_i^j$ should be maintained between the normalized actual pointing direction vector $\boldsymbol{y}'_{i,c}$ and the normalized vector $\boldsymbol{x}_j$ pointing toward a certain bright object and represented in the inertial frame $\mathcal{I}$, i.e., $\beta_i^j > (\theta_g)_i^j$ with $0 < (\theta_g)_i^j < \pi$. The index j represents the j-th celestial objects associated with the i-th airborne equipment. This constraint can be expressed by

$$\boldsymbol{x}_j \cdot \boldsymbol{y}'_{i,c} < \cos((\theta_g)_i^j), \quad (6)$$

Combining (6) and (5) yields

$$\begin{aligned}2\boldsymbol{q}^T\boldsymbol{y}_{i,c}\boldsymbol{q}^T\boldsymbol{x}_j - \boldsymbol{q}^T\boldsymbol{q}\boldsymbol{x}_j^T\boldsymbol{y}_{i,c} + q_0^2\boldsymbol{x}_j^T\boldsymbol{y}_{i,c} \\ + 2q_0\boldsymbol{q}^T(\boldsymbol{x}_j \times \boldsymbol{y}_{i,c}) < \cos((\theta_g)_i^j).\end{aligned} \quad (7)$$

Note that the nominal pointing direction $\boldsymbol{y}_i$ of airborne equipment may have a deviation $\Delta\boldsymbol{y}_i$. Then the actual pointing direction is $\boldsymbol{y}_{i,c} = \boldsymbol{y}_i + \Delta\boldsymbol{y}_i$.

Assumption 2: The deviation $\Delta\boldsymbol{y}_i$ is bounded by $\|\Delta\boldsymbol{y}_i\| \leq \varepsilon_i < 1$, where ε_i is a positive constant.

Since the deviation is caused by external disturbances, installation errors, vibrations and measurement errors, it is reasonable to assume that this deviation is upper bounded by a small constant ε_i being less than 1. Moreover, let δ_i denote the angle between $\boldsymbol{y}_{i,c}$ and $\boldsymbol{y}_i$ of the i-th sensitive equipment represented in the body frame. Then, the following lemma holds:

Lemma 1: If Assumption 2 holds, δ_i is bounded by a constant, i.e., $0 \leq \delta_i \leq \delta_{i,\max}$ with $\delta_{i,\max} = \arcsin(\varepsilon_i)$.

Proof: As shown in Fig, 2(a), three vectors $\boldsymbol{y}_i$, $\Delta\boldsymbol{y}_i$, $\boldsymbol{y}_i + \Delta\boldsymbol{y}_i$ form a triangle. Because $\|\Delta\boldsymbol{y}_i\| \leq \varepsilon_i$, $\Delta\boldsymbol{y}_i$ can only be in a sphere of radius ε_i. In addition, since $\|\Delta\boldsymbol{y}_i\| < 1$, δ_i,

$0 \le \delta_i < \frac{\pi}{2}$. Let σ_i be the angle between $\Delta \boldsymbol{y}_i$ and $\boldsymbol{y}_i + \Delta \boldsymbol{y}_i$. Then, in view of the law of sines, we have

$$\frac{\|\boldsymbol{y}_i\|}{\sin(\sigma_i)} = \frac{\|\Delta \boldsymbol{y}_i\|}{\sin(\delta_i)} \le \frac{\varepsilon_i}{\sin(\delta_i)}. \tag{8}$$

Since $0 \le \delta_i < \frac{\pi}{2}$, $\sin(\delta_i) > 0$ and $\|\boldsymbol{y}_i\| = 1$, we have $\sin(\delta_i) \le \varepsilon_i \sin(\sigma_i)$ from (8). Due to the facts that $\max_{\sigma_i} \sin(\sigma_i) = 1$ and $\sin(\delta_i)$ is monotonically increasing, the allowable maximum value of δ_i is obtained as

$$\delta_{i,\max} = \arcsin(\varepsilon_i) \tag{9}$$

when $\sigma_i = \frac{\pi}{2}$. This completes the proof. ■

Based on Lemma 1, we further have the following lemma.

Lemma 2: Considering the deviation of airborne equipment, the angle requirement of constrained zones $\mathrm{ang}(\boldsymbol{x}_j, \boldsymbol{y}'_{i,c}) > (\theta_g)_i^j$ is equivalent to $\mathrm{ang}(\boldsymbol{x}_j, \boldsymbol{y}'_i) > (\theta_g)_i^j + \arcsin(\varepsilon_i)$, where $(\theta_g)_i^j$ is the known constant angle constraint and the function $\mathrm{ang}(\boldsymbol{a}, \boldsymbol{b})$ represents the angle between vectors $\boldsymbol{a}$ and $\boldsymbol{b}$.

Proof: To satisfy $\mathrm{ang}(\boldsymbol{x}_j, \boldsymbol{y}'_{i,c}) > (\theta_g)_i^j$ for any deviations, we have to ensure

$$\min_{0 \le \delta_i \le \delta_{i,\max}} \mathrm{ang}(\boldsymbol{x}_j, \boldsymbol{y}'_{i,c}) > (\theta_g)_i^j. \tag{10}$$

In view of the trigonometric inequality, it is clear that

$$\min_{0 \le \delta_i \le \delta_{i,\max}} \mathrm{ang}(\boldsymbol{x}_j, \boldsymbol{y}'_{i,c}) = \mathrm{ang}(\boldsymbol{x}_j, \boldsymbol{y}'_i) - \delta_{i,\max}. \tag{11}$$

Therefore, we have $\mathrm{ang}(\boldsymbol{x}_j, \boldsymbol{y}'_i) > (\theta_g)_i^j + \arcsin(\varepsilon_i)$ according to Lemma 1. This completes the proof. ■

Then the constraint (7) can be further written as [6]

$$\boldsymbol{Q}^T \boldsymbol{M}_i^j \boldsymbol{Q} < 0, \tag{12}$$

where for $i = 1, \ldots, n$ and $j = 1, \ldots, m$,

$$\begin{aligned} \boldsymbol{M}_i^j &= \begin{bmatrix} \boldsymbol{A}_i^j & \boldsymbol{b}_i^j \\ \boldsymbol{b}_i^{jT} & d_i^j \end{bmatrix}, \boldsymbol{b}_i^j = \boldsymbol{x}_j \times \boldsymbol{y}_i, \\ \boldsymbol{A}_i^j &= \boldsymbol{x}_j \boldsymbol{y}_i^T + \boldsymbol{y}_i \boldsymbol{x}_j^T \\ &\quad - (\boldsymbol{x}_j^T \boldsymbol{y}_i + \cos((\theta_g)_i^j + \arcsin(\varepsilon_i))) \boldsymbol{I}_3, \\ d_i^j &= \boldsymbol{x}_j^T \boldsymbol{y}_i - \cos((\theta_g)_i^j + \arcsin(\varepsilon_i)). \end{aligned} \tag{13}$$

As a result, for the i-th sensitive instrument subject to pointing direction deviations, the set of attitudes $\boldsymbol{Q}_{F_i^j} \subseteq \mathbb{Q}_u$ that avoids the j-th constrained zone can be represented as

$$\boldsymbol{Q}_{F_i^j} = \left\{ \boldsymbol{Q} \in \mathbb{Q}_u \mid \boldsymbol{Q}^T \boldsymbol{M}_i^j(\theta_i^j) \boldsymbol{Q} < 0 \right\}, \tag{14}$$

where $\theta_i^j = (\theta_g)_i^j + \arcsin(\varepsilon_i)$. In general, the attitude constrained zones are defined for all n on-board sensitive instruments and the associated m constraint objects.

Moreover, we define the warning angle to specify when attitude constrained zones need to be taken into consideration.

Definition 2 (Warning Angle): Consider that the spacecraft rotates toward to the constrained zone about its major principal axis with inertia $J_{\max}$, the initial pointing direction is $\boldsymbol{y}'_{i,0}$, and initial angular velocity is the allowable maximum angular velocity $\omega_{\max}$. As shown in Fig. 2b, if the maximum torque $u_{\max}$ is applied to decelerate the spacecraft such that the angular velocity reduces to zero at the moment that the pointing direction reaches the nearest boundary $\boldsymbol{y}'_{i,f}$ of the constrained zone, then the warning angle $(\theta_w)_i^j$ can be defined as the angle between $\boldsymbol{y}'_{i,0}$ and $\boldsymbol{x}_j$.

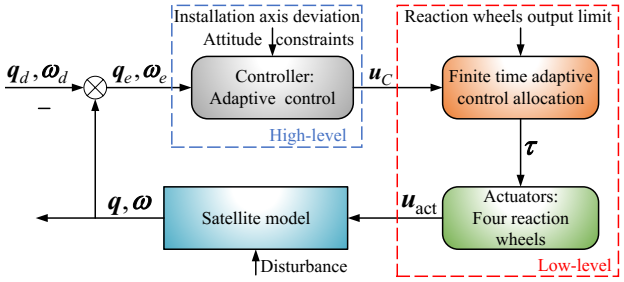

Fig. 3: The overall schematic diagram of control system.

According to Definition 2 and Lemma 2, we have

$$(\theta_g)_i^j + \arcsin(\varepsilon_i) = \frac{1}{2} \frac{u_{\max}}{J_{\max}} (t_f - t_0)^2 - \omega_{\max} (t_f - t_0) + (\theta_w)_i^j$$

where t_0 and t_f represent the initial time instant and the warning time instant that the pointing direction reaches the nearest boundary of attitude constrained zone, respectively. Solving above equation such that $t_f - t_0$ has a unique solution, the warning angle can be obtained as

$$(\theta_w)_i^j = \frac{1}{2} \frac{J_{\max}}{u_{\max}} \omega_{\max}^2 + (\theta_g)_i^j + \arcsin(\varepsilon_i). \tag{15}$$

Remark 1: According to [6], if the attitude $\boldsymbol{Q} \in \boldsymbol{Q}_{F_i^j}$, then we further have $-2 < \boldsymbol{Q}^T \boldsymbol{M}_i^j(\theta_i^j) \boldsymbol{Q} < 0$. Specifically, $\boldsymbol{Q}^T \boldsymbol{M}_i^j(\theta_i^j) \boldsymbol{Q} = 0$ indicates that the pointing direction of the sensitive equipment is on the boundary of the attitude constrained zone, while $\boldsymbol{Q}^T \boldsymbol{M}_i^j(\theta_i^j) \boldsymbol{Q} = -2$ means that the pointing direction of sensitive instrument is far away from the constrained zone. In light of the warning angle in Definition 2, we set $\boldsymbol{Q}^T \boldsymbol{M}_i^j(\theta_i^j) \boldsymbol{Q} = -2$ when $\mathrm{ang}(\boldsymbol{x}_j, \boldsymbol{y}'_i) > (\theta_w)_i^j$.

III. Problem Statement

The overall diagram of attitude control system is shown in Fig. 3. In design process, two problems are to be solved:

Problem 1: [High-level controller] Under attitude constraints and instrument pointing direction deviation, design an attitude controller to complete the attitude reorientation.

Problem 2: [Control allocation] Considering output limitation of actuator, design a finite-time adaptive CA to realize the commanded control action from high-level controller.

IV. High-Level Controller

In this section, we solve Problem 1 by designing a robust potential function-based adaptive attitude controller.

A. Robust Potential Function

In view of warning angle (cf. Definition 2), we define the operating set Ω.

Definition 3 (Constraint Operating Set): The constraint operating set is defined as $\Omega \triangleq \{(i,j) \mid \theta_i^j < \mathrm{ang}(\boldsymbol{x}_j, \boldsymbol{y}'_i) < (\theta_w)_i^j\}$, which is a collection of (i,j) pairs satisfying the condition $\theta_i^j < \mathrm{ang}(\boldsymbol{x}_j, \boldsymbol{y}'_i) < (\theta_w)_i^j$ for all $i = 1, \ldots, n$ and $j = 1, \ldots, m$.

Based on Definition 3 and Remark 1, the operating set indicates constrained zones considered in potential function. Now, a logarithmic potential function V_1 is proposed as

$$V_1(\boldsymbol{Q})=\|\boldsymbol{Q}_d-\boldsymbol{Q}\|^2\left[\sum_{(i,j)\in\Omega}-\alpha\log\left(-\frac{\boldsymbol{Q}^T\boldsymbol{M}_i^j(\theta_i^j)\boldsymbol{Q}}{2}\right)\right], \quad (16)$$

where α is a positive constant. Since the pointing direction deviation of sensitive instrument is considered in the potential function design, the proposed potential function (16) has stronger robustness than that in [6]–[9]. Moreover, the proposed potential function is synthesized by only using pairs in the operating set, and hence avoids considering constrained zones that are far away from sensitive instruments. In addition, the proposed robust potential function is also convex with respect to $\boldsymbol{Q}$, which can be found in Proposition 6 of [6].

B. Adaptive Controller Design

Motived by [9], the high-level controller is designed as

$$\begin{aligned}\boldsymbol{u}_C=&-k_2\boldsymbol{s}+\boldsymbol{S}(\boldsymbol{\omega})\boldsymbol{J}\boldsymbol{\omega}-\frac{k_1}{2}\boldsymbol{J}[\boldsymbol{S}(\boldsymbol{q}_e)+q_{e0}\boldsymbol{I}_3]\boldsymbol{\omega}\\&-k_1k_3{\boldsymbol{q}_e}^T\mathrm{Vec}[(\nabla V_1^*\otimes\boldsymbol{Q})]\frac{\boldsymbol{s}}{\|\boldsymbol{s}\|^2}\\&+k_3\mathrm{Vec}[(\nabla V_1^*\otimes\boldsymbol{Q})]-\hat{\boldsymbol{d}}\frac{\boldsymbol{s}}{\|\boldsymbol{s}\|^2}\end{aligned} \quad (17)$$

with

$$\dot{\hat{\boldsymbol{d}}}=\rho[\|\boldsymbol{s}\|-\mu(\hat{\boldsymbol{d}}-\hat{\boldsymbol{d}}_{\max})],\ \dot{\hat{\boldsymbol{d}}}_{\max}=\delta(\hat{\boldsymbol{d}}-\hat{\boldsymbol{d}}_{\max}), \quad (18)$$

where $\boldsymbol{s}=[s_1,s_2,s_3]^T\in\mathbb{R}^3$ is a sliding vector defined as $\boldsymbol{s}=\boldsymbol{\omega}+k_1\boldsymbol{q}_e$, k_1, k_2, k_3, ρ, μ, δ are positive constants. The stability of the closed-loop system with the above adaptive sliding mode controller is summarized in the following theorem.

Theorem 1: Consider the attitude kinematics and dynamics expressed by (2) and (3). The high-level attitude controller (17) with adaptive law (18) solves Problem 1 such that all closed-loop signals are bounded and that $\lim_{t\to\infty}\boldsymbol{q}_e(t)=0$ and $\lim_{t\to\infty}\boldsymbol{\omega}(t)=0$ despite the existence of attitude-constrained zones and instrument pointing direction deviations.

Proof: Consider the following Lyapunov candidate:

$$\begin{aligned}V_C=&2k_1k_2\left({\boldsymbol{q}_e}^T\boldsymbol{q}_e+(1-q_{e0})^2\right)+2k_3V_1+\frac{1}{2}\boldsymbol{s}^T\boldsymbol{J}\boldsymbol{s}\\&+\frac{1}{2\rho}\left(\hat{\boldsymbol{d}}-\boldsymbol{d}_{\max}\right)^2+\frac{\mu}{2\delta}\left(\hat{\boldsymbol{d}}_{\max}-\boldsymbol{d}_{\max}\right)^2.\end{aligned} \quad (19)$$

The time derivative of V_C is

$$\begin{aligned}\dot{V}_C=&2k_1k_2{\boldsymbol{q}_e}^T\boldsymbol{\omega}+2k_3\nabla V_1^T\left[\frac{1}{2}\boldsymbol{Q}\otimes\boldsymbol{v}(\boldsymbol{\omega})\right]+\boldsymbol{s}^T\boldsymbol{J}\dot{\boldsymbol{s}}\\&+\frac{1}{\rho}\left(\hat{\boldsymbol{d}}-\boldsymbol{d}_{\max}\right)\dot{\hat{\boldsymbol{d}}}+\frac{\mu}{\delta}\left(\hat{\boldsymbol{d}}_{\max}-\boldsymbol{d}_{\max}\right)\dot{\hat{\boldsymbol{d}}}_{\max}.\end{aligned} \quad (20)$$

Then, using $k_3\nabla V_1^T[\boldsymbol{Q}\otimes\boldsymbol{v}(\boldsymbol{\omega})]=-k_3\boldsymbol{\omega}^T\mathrm{Vec}[\nabla V_1^*\otimes\boldsymbol{Q}]$ and substituting the controller (17) and adaptive law (18) into the above equation yields

$$\dot{V}_C\le-k_2\|\boldsymbol{\omega}\|^2-{k_1}^2k_2\|\boldsymbol{q}_e\|^2, \quad (21)$$

which leads to $\lim_{t\to\infty}\boldsymbol{q}_e(t)=0$ and $\lim_{t\to\infty}\boldsymbol{\omega}(t)=0$. ■

V. Finite-Time Adaptive Control Allocation

Consider that the high-level controller (17) and $N>3$ actuators are used. The CA problem is formulated as

$$\begin{aligned}\min_{\boldsymbol{\tau}}\quad&J_e=\frac{1}{2}\boldsymbol{\tau}^T\boldsymbol{W}_v\boldsymbol{\tau}\\\text{s.t.}\quad&\boldsymbol{D}\boldsymbol{\tau}=\boldsymbol{u}_C,\\&\tau_{i,\min}\le\tau_i\le\tau_{i,\max},\quad i=1,\dots,N\end{aligned} \quad (22)$$

where $\boldsymbol{W}_v$ is a positive definite weighting matrix and $\tau_{i,\min}$ and $\tau_{i,\max}$ are constants representing the lower and upper bounds of saturation limits of each actuator. To solve the constrained optimization problem in (22), we introducing a Lagrange multiplier $\boldsymbol{\lambda}=[\lambda_1,\lambda_2,\lambda_3]^T\in\mathbb{R}^3$ and define the corresponding Lagrangian function as

$$\begin{aligned}L(\boldsymbol{u_C},\boldsymbol{\tau},\boldsymbol{\lambda})=&\frac{1}{2}\boldsymbol{\tau}^T\boldsymbol{W}_v\boldsymbol{\tau}-p\sum_{l=1}^{2}\sum_{i=1}^{N}\ln\left(C_{l,i}(\tau_i)\right)\\&+(\boldsymbol{u}_C-\boldsymbol{D}\boldsymbol{\tau})^T\boldsymbol{\lambda},\end{aligned} \quad (23)$$

where p is a positive constant defining the barrier function slopes, the functions $C_{1,i}=\tau_i-\tau_{i,\min}$ and $C_{2,i}=\tau_{i,\max}-\tau_i$ for all $i\in\{1,\dots,N\}$. Consequently, the CA problem (22) is reformulated as an unconstrained optimization problem:

$$\min_{\boldsymbol{\tau},\boldsymbol{\lambda}}L(\boldsymbol{u}_C,\boldsymbol{\tau},\boldsymbol{\lambda}). \quad (24)$$

Define the first-order optimal set of Eq.(24) as

$$\mathcal{Z}=\left\{\left(\boldsymbol{\tau}^T,\boldsymbol{\lambda}^T\right)^T\mid\left(\left(\frac{\partial L}{\partial\boldsymbol{\tau}}\right)^T,\left(\frac{\partial L}{\partial\boldsymbol{\lambda}}\right)^T\right)^T=0\right\}, \quad (25)$$

where

$$\frac{\partial L}{\partial\boldsymbol{\tau}}=\boldsymbol{W}_v^T\boldsymbol{\tau}-\boldsymbol{D}^T\boldsymbol{\lambda}-p\left(\boldsymbol{\tau}_{r,\min}-\boldsymbol{\tau}_{r,\max}\right),\ \frac{\partial L}{\partial\boldsymbol{\lambda}}=\boldsymbol{u}_C-\boldsymbol{D}\boldsymbol{\tau} \quad (26)$$

with $\boldsymbol{\tau}_{r,\min}\triangleq\left[\frac{1}{\tau_1-\tau_{1,\min}},\dots,\frac{1}{\tau_N-u_{N,\min}}\right]^T\in\mathbb{R}^N$ and $\boldsymbol{\tau}_{r,\max}\triangleq\left[\frac{1}{\tau_{1,\max}-\tau_1},\dots,\frac{1}{\tau_{N,\max}-\tau_N}\right]^T\in\mathbb{R}^N$. The first equation $\frac{\partial L}{\partial\boldsymbol{\tau}}=0$ ensures the actuator saturation constraint. The second equation $\frac{\partial L}{\partial\boldsymbol{\lambda}}=0$ guarantees the equality constraint in original CA problem.

Lemma 3: The CA problem (24) achieves local minima if and only if the first-order optimal set $\mathcal{Z}$ is reached.

Proof: Necessity: If the set $\mathcal{Z}$ is reached, then it is clear that the CA problem in (24) achieves its local minima.

Sufficiency: In view of (26), if $\frac{\partial L}{\partial\boldsymbol{\lambda}}=0$, we have $\boldsymbol{u}_C=\boldsymbol{D}\boldsymbol{\tau}$, implying the equality constraint in original CA problem is satisfied. Moreover, the Lagrangian function defined in (23) is independent of $\boldsymbol{\lambda}$ when $\frac{\partial L}{\partial\boldsymbol{\lambda}}=0$. In this case, based on the second-order sufficient condition [17], the local minima is achieved if $\frac{\partial L}{\partial\boldsymbol{\tau}}=0$ and $\frac{\partial^2L}{\partial\boldsymbol{\tau}^2}>0$. From (26), we have

$$\frac{\partial^2L}{\partial\boldsymbol{\tau}^2}=\boldsymbol{W}_v^T+p\,\mathrm{diag}\left\{\boldsymbol{\tau}_{r^2,\min}+\boldsymbol{\tau}_{r^2,\max}\right\}, \quad (27)$$

where $\boldsymbol{\tau}_{r^2,\min}\triangleq\left[\frac{1}{(\tau_1-\tau_{1,\min})^2},\dots,\frac{1}{(\tau_N-\tau_{\min})^2}\right]^T\in\mathbb{R}^N$ and $\boldsymbol{\tau}_{r^2,\max}\triangleq\left[\frac{1}{(\tau_{1,\max}-\tau_1)^2},\dots,\frac{1}{(\tau_{N,\max}-\tau_N)^2}\right]^T\in\mathbb{R}^N$. Since the second term of (27) is a positive-definite diagonal matrix, we have $\frac{\partial^2L}{\partial\boldsymbol{\tau}^2}>0$. Hence, the sufficiency is ensured. ■

Then, motived by [14], a dynamic update law for calculating the optimal parameters $\boldsymbol{\tau}$ and $\boldsymbol{\lambda}$ is proposed as

$$\begin{bmatrix} \dot{\boldsymbol{\tau}} \\ \dot{\boldsymbol{\lambda}} \end{bmatrix} = -k_4 \boldsymbol{G}^{-1} \operatorname{sig}\begin{pmatrix} \frac{\partial L}{\partial \boldsymbol{\tau}} \\ \frac{\partial L}{\partial \boldsymbol{\lambda}} \end{pmatrix} + \boldsymbol{\phi}, \tag{28}$$

where

$$\boldsymbol{G} = \begin{bmatrix} \frac{\partial^2 L}{\partial \boldsymbol{\tau}^2} & \frac{\partial^2 L}{\partial \boldsymbol{\tau} \partial \boldsymbol{\lambda}} \\ \frac{\partial^2 L}{\partial \boldsymbol{\lambda} \partial \boldsymbol{\tau}} & 0 \end{bmatrix} \tag{29}$$

$$\operatorname{sig}(\boldsymbol{x}) = \left[|x_1|^\gamma \operatorname{sgn}(x_1), \cdots, |x_{N+3}|^\gamma \operatorname{sgn}(x_{N+3})\right]^T \tag{30}$$

with $0 < \gamma < 1$, $\boldsymbol{\phi} \in \mathbb{R}^{N+3}$ satisfies the following equation

$$\left[\left(\frac{\partial L}{\partial \boldsymbol{\tau}}\right)^T \quad \left(\frac{\partial L}{\partial \boldsymbol{\lambda}}\right)^T\right] \boldsymbol{G}\boldsymbol{\phi} + \boldsymbol{z} = 0, \tag{31}$$

where the auxiliary parameter $\boldsymbol{z}$ is defined as

$$\boldsymbol{z} = \left(\frac{\partial L}{\partial \boldsymbol{\lambda}}\right)^T \frac{\partial^2 L}{\partial \boldsymbol{u}_C \partial \boldsymbol{\lambda}} \dot{\boldsymbol{u}}_C. \tag{32}$$

Remark 2: To calculate $\boldsymbol{\phi}$ from (31), we can solve a least-square problem. Define a new Lagrangian function

$$L_a(\boldsymbol{\phi}, \lambda_a) = \frac{1}{2}\boldsymbol{\phi}^T\boldsymbol{\phi} + \boldsymbol{\lambda}_a\left(\left[\left(\frac{\partial L}{\partial \boldsymbol{\tau}}\right)^T \quad \left(\frac{\partial L}{\partial \boldsymbol{\lambda}}\right)^T\right]\boldsymbol{G}\boldsymbol{\phi} + \boldsymbol{z}\right) \tag{33}$$

where $\boldsymbol{\lambda}_a$ is a Lagrangian multiplier. Through first-order optimality conditions $\frac{\partial L_a}{\partial \boldsymbol{\phi}} = 0$ and $\frac{\partial L_a}{\partial \lambda_a} = 0$, we have

$$\begin{bmatrix} \boldsymbol{I}_{N+3} & \boldsymbol{G}^T\begin{bmatrix}\left(\frac{\partial L}{\partial \boldsymbol{\tau}}\right) \\ \left(\frac{\partial L}{\partial \boldsymbol{\lambda}}\right)\end{bmatrix} \\ \left[\left(\frac{\partial L}{\partial \boldsymbol{\tau}}\right)^T \quad \left(\frac{\partial L}{\partial \boldsymbol{\lambda}}\right)^T\right]\boldsymbol{G} & 0 \end{bmatrix} \begin{bmatrix} \boldsymbol{\phi} \\ \lambda_a \end{bmatrix} = \begin{bmatrix} 0 \\ -\boldsymbol{z} \end{bmatrix}. \tag{34}$$

Note that the above equation always has a unique solution for $\boldsymbol{\phi}$ when $[(\frac{\partial L}{\partial \boldsymbol{\tau}})^T(\frac{\partial L}{\partial \boldsymbol{\lambda}})^T]\boldsymbol{G} \neq 0$.

Now, we are ready to present the main result of the proposed finite time adaptive control allocation and its solution.

Theorem 2: The update law (28) solves Problem 2, leading to that $\left(\boldsymbol{\tau}^T, \boldsymbol{\lambda}^T\right)^T \to \mathcal{Z}$ in finite time.

Proof: Select a Lyapunov-like function as

$$V_2(\boldsymbol{u}_C, \boldsymbol{\tau}, \boldsymbol{\lambda}) = \frac{1}{2}\left(\left(\frac{\partial L}{\partial \boldsymbol{\tau}}\right)^T \frac{\partial L}{\partial \boldsymbol{\tau}} + \left(\frac{\partial L}{\partial \boldsymbol{\lambda}}\right)^T \frac{\partial L}{\partial \boldsymbol{\lambda}}\right). \tag{35}$$

According to (28) and (31), $\frac{\partial^2 L}{\partial \boldsymbol{u}_C \partial \boldsymbol{\tau}} = 0$ and $\frac{\partial^2 L}{\partial \boldsymbol{\lambda}^2} = 0$. Then, the time derivative of $V_2(\boldsymbol{u}_C, \boldsymbol{\tau})$ is

$$\dot{V}_2 = -k_4\left[\left(\frac{\partial L}{\partial \boldsymbol{\tau}}\right)^T \quad \left(\frac{\partial L}{\partial \boldsymbol{\lambda}}\right)^T\right] \operatorname{sig}\left(\begin{bmatrix}\frac{\partial L}{\partial \boldsymbol{\tau}} \\ \frac{\partial L}{\partial \boldsymbol{\lambda}}\end{bmatrix}\right) \leq -2^{\frac{\gamma+1}{2}} k_4 V_2^{\frac{\gamma+1}{2}}. \tag{36}$$

Therefore, based on Theorem 4.2 of [18], the optimal set $\mathcal{Z}$ is reached in finite time, and the reaching time is

$$T_{\text{reach}} \leq \frac{V_2^{\frac{1-\gamma}{2}}(\boldsymbol{u}_C(0), \boldsymbol{\tau}(0), \boldsymbol{\lambda}(0))}{2^{\frac{1-\gamma}{2}}\beta(1-\gamma)}. \tag{37}$$

Thus, the proof can be completed by showing $\boldsymbol{G}$ in (28) is nonsingular. In view of (27), we obtain $\frac{\partial^2 L}{\partial \boldsymbol{\tau}^2}$ is positive-definite and nonsingular. Then, the determinant of $\boldsymbol{G}$ is

$$\det(\boldsymbol{G}) = \det\left(\frac{\partial^2 L}{\partial \boldsymbol{\tau}^2}\right) \det\left(-\boldsymbol{D}^T\left(\frac{\partial^2 L}{\partial \boldsymbol{\tau}^2}\right)^{-1}\boldsymbol{D}\right), \tag{38}$$

where $\boldsymbol{D}$ is the installation position of actuators, which is positive-definite and nonsingular. Therefore, it is clear that $\det(\boldsymbol{G}) \neq 0$, i.e., the matrix $\boldsymbol{G}$ is nonsingular. ■

TABLE I: Control parameters chosen

Control schemes	Control gains
Controller (17) using proposed potential function in (16) or potential function in [6]	$k_1 = 0.056$, $k_2 = 0.4853\boldsymbol{J}$, $k_3 = 0.1422\boldsymbol{J}$, $\alpha = 0.01$ $\rho = 0.005$, $\mu = 0.1$, $\delta = 0.5$
PD controller [19]	$k_p = 0.0272\boldsymbol{J}$, $k_d = 0.4853\boldsymbol{J}$

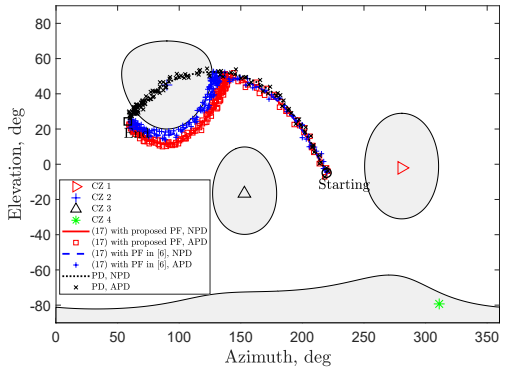

Fig. 4: Trajectories of sensitive instrument pointing direction in 2-D cylindrical projection. (PF: potential function, NPD: nominal pointing direction, APD: actual pointing direction)

VI. Simulation Results

The inertia of spacecraft is $\boldsymbol{J} = \operatorname{diag}([20, 15, 20])$ kg·m^2. The environmental disturbance is assumed to be same as in [9]. The spacecraft carries a light-sensitive instrument with a fixed boresight vector in the spacecraft body axis $\boldsymbol{y}$, and the deviation $\Delta\boldsymbol{y} = [\Delta y_1, \Delta y_2, \Delta y_3]^T \in \mathbb{R}^3$ caused by inaccurate installation or vibration is $\Delta y_k = 0.045\text{rand}(\Delta t_k)$ for $k \in \{1, 2, 3\}$, where the output of function $\text{rand}(\Delta t_k)$ is a random number in interval $[-1, 1]$ every Δt_k and 0 otherwise. In simulation, we set $\Delta t_k = 1$ s. Then, based on (9), we have $\delta_{\max} = \arcsin(0.078) = 4.4658$ deg. Four reaction wheels with distribution matrix $\boldsymbol{D} = \frac{1}{\sqrt{3}}[-1, -1, 1, 1; 1, -1, -1, 1; 1, 1, 1, 1]$ are used and limited by $|\tau_i| \leq 0.2$ N·m for $i = 1, \ldots 4$, so the high-level controller satisfies $\|\boldsymbol{u}\| \leq 0.5774$ N·m. Moreover, the angular velocity is limited by $\|\boldsymbol{\omega}\| \leq 8.66$ deg/s.

Four attitude constrained zones (i.e., CZ 1-CZ 4 in Fig. 4) are considered and their details can be found in [6]. The warning angles of four constrained zones are $(\theta_w)_1^1 = 57.15$ deg, $(\theta_w)_1^2 = 52.15$ deg, $(\theta_w)_1^3 = 52.15$ deg and $(\theta_w)_1^4 = 47.15$ deg. Initial attitude is $\boldsymbol{Q}(0) = [0.33, 0.66, -0.62, -0.2726]^T$ and initial angular velocity is $\boldsymbol{\omega}(0) = [0, 0, 0]^T$ deg/s. The desired attitude is set as $\boldsymbol{Q}_d = [0.2, -0.5, -0.5, -0.6782]^T$, which lies outside of four attitude constrained zones.

A. High-Level Virtual Controller Comparison

Here, we verify the proposed high-level controller. For comparison, in addition to the controller (17) using the proposed potential function (16), the controller (17) using potential function in [6] without considering pointing deviation, and PD controller in [19] are also simulated. Table I shows gains of the three controllers. In this subsection, the virtual control torque is directly acted on spacecraft.

Trajectories of nominal and deviated/actual instrument pointing direction in 2-D projection are shown in Fig. 4. It is clear that both nominal and deviated pointing trajectories

TABLE II: Control allocation parameters chosen

Control allocation schemes	Parameters
Proposed FTACA in (28)	$k_4 = 1.5$, $\gamma = 0.65$ $\boldsymbol{W}_v = 0.05\boldsymbol{I}_3$, $p = 0.008$
ACA in [16]	$\Gamma = 1.5$, $W = 1.5$, $\boldsymbol{W}_v = 0.05\boldsymbol{I}_3$, $p = 0.008$
PICA	$\boldsymbol{\tau} = \boldsymbol{D}^T(\boldsymbol{D}\boldsymbol{D}^T)^{-1}\boldsymbol{u}_C$

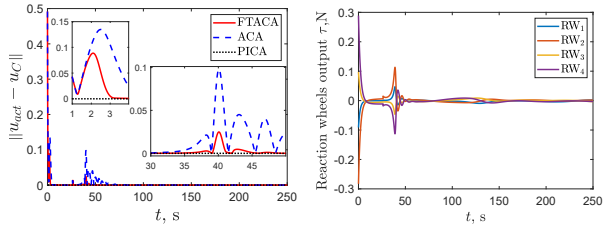

(a) Control allocation error

(b) Actuator output $\boldsymbol{\tau}$ with PICA

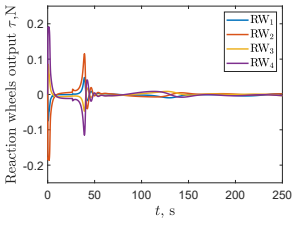

(c) Actuator output $\boldsymbol{\tau}$ with FTACA

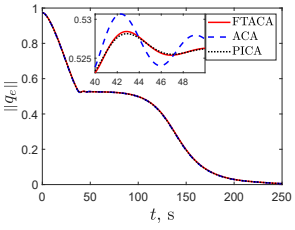

(d) $\|\boldsymbol{q}_e\|$

Fig. 5: Comparison of three control allocation methods.

using the PD controller violate attitude constraints. Although the nominal pointing direction using controller (17) with potential function in [6] can avoid the four attitude constraints, the actual pointing direction enters into constrained zones occasionally since the potential function in [6] does not consider pointing direction deviations. In contrast, the proposed potential function-based controller guarantees attitude constraints for both the nominal and actual pointing trajectories. Moreover, the controller using the proposed potential function may spend more time and control efforts than that using potential function in [6] due to the introduction of robustness.

B. Control Allocation Comparison

This subsection verifies the efficiency of the proposed finite-time adaptive CA (FTACA) approach in (28). Two other existing CA methods, i.e., adaptive CA (ACA) in [16] and pseudoinverse-based CA (PICA), are also implemented for comparison. Table II shows parameters of these three CA methods. Controller (17) with proposed potential function (16) is used for all three CA methods.

As seen from Fig. 5a, the CA error $\|\boldsymbol{u}_{act} - \boldsymbol{u}_C\|$ can converge to zero asymptotically by the proposed FTACA and ACA, where $\boldsymbol{u}_{act}$ is the actual output of actuators. However, the proposed one requires less convergence time. Moreover, the CA error under PICA is always close to zero since it solves the CA problem exactly and does not consider saturation constraint. The actuator outputs of the proposed control allocation and the PICA are depicted in Fig. 5b-5c, from which it is clear that both FTACA scheme satisfies the actuator saturation constraint, while the PICA scheme cannot. Fig. 5d demonstrates that the required attitude reorientation can be achieved by all three CA schemes.

VII. Conclusions

In this paper, a finite-time CA-based attitude controller for spacecraft subject to attitude-constrained zones and pointing direction deviation of sensitive instrument is proposed. A high-level adaptive controller using a warning angle-based robust potential function is designed to realize rest-to-rest attitude maneuver and avoid attitude constraints. In addition, we also designed a finite-time adaptive control allocation approach to distribute desired control actions to actuators dynamically. Simulation results verify the proposed overall attitude control scheme. Future work includes extending the proposed potential function to intersected constrained zones.

References

[1] R. Kristiansen, P. J. Nicklasson, and J. T. Gravdahl, "Spacecraft coordination control in 6DOF: Integrator backstepping vs passivity-based control," *Automatica*, vol. 44, no. 11, pp. 2896–2901, 2008.

[2] Q. Shen, D. Wang, S. Zhu, and E. K. Poh, "Integral-type sliding mode fault-tolerant control for attitude stabilization of spacecraft," *IEEE Transactions on Control Systems Technology*, vol. 23, no. 3, pp. 1131–1138, 2015.

[3] S. D. Gennaro, "Output stabilization of flexible spacecraft with active vibration suppression," *IEEE Transactions on Aerospace and Electronic Systems*, vol. 39, no. 3, pp. p.747–759, 2003.

[4] W. Luo, Y.-C. Chu, and K.-V. Ling, "Inverse optimal adaptive control for attitude tracking of spacecraft," *IEEE Transactions on Automatic Control*, vol. 50, no. 11, pp. 1639–1654, 2005.

[5] E. L. D. Angelis, F. Giulietti, and G. Avanzini, "Single-axis pointing of underactuated spacecraft in the presence of path constraints," *Journal of Guidance Control and Dynamics*, vol. 38, no. 1, pp. 143–147, 2015.

[6] U. Lee and M. Mesbahi, "Feedback control for spacecraft reorientation under attitude constraints via convex potentials," *IEEE Transactions on Aerospace and Electronic Systems*, vol. 50, no. 4, pp. 2578–2592, 2014.

[7] C. R. Mclnnes, "Large angle slew maneuvers with autonomous sun vector avoidance," *Journal of Guidance Control and Dynamics*, vol. 17, no. 4, pp. 875–877, 1994.

[8] Q. Shen, C. Yue, and C. H. Goh, "Velocity-free attitude reorientation of a flexible spacecraft with attitude constraints," *Journal of Guidance Control and Dynamics*, vol. 40, no. 5, pp. 1293–1299, 2017.

[9] Q. Shen, C. Yue, C. H. Goh, B. Wu, and D. Wang, "Rigid-body attitude stabilization with attitude and angular rate constraints," *Automatica*, vol. 90, pp. 157–163, 2018.

[10] H. Alwi and C. Edwards, "Fault tolerant control using sliding modes with on-line control allocation," *Automatica*, vol. 44, no. 7, pp. 1859–1866, 2008.

[11] Q. Shen, D. Wang, S. Zhu, and E. K. Poh, "Inertia-free fault-tolerant spacecraft attitude tracking using control allocation," *Automatica*, vol. 62, no. C, pp. 114–121, 2015.

[12] Q. Hu, B. Li, D. Wang, and E. K. Poh, "Velocity-free fault-tolerant control allocation for flexible spacecraft with redundant thrusters," *International Journal of Systems Science*, vol. 46, no. 6, pp. 976–992, 2015.

[13] T. A. Johansen and T. I. Fossen, "Control allocation—a survey," *Automatica*, vol. 49, no. 5, pp. 1087–1103, 2013.

[14] J. Tjønnås and T. A. Johansen, "Adaptive control allocation," *Automatica*, vol. 44, no. 11, pp. 2754–2765, 2008.

[15] Y. Chen and J. Wang, "Adaptive energy-efficient control allocation for planar motion control of over-actuated electric ground vehicles," *IEEE Transactions on Control Systems Technology*, vol. 22, no. 4, pp. 1362–1373, 2014.

[16] Q. Hu and X. Tan, "Dynamic near-optimal control allocation for spacecraft attitude control using a hybrid configuration of actuators," *IEEE Transactions on Aerospace and Electronic Systems*, vol. 56, no. 2, pp. 1430–1443, 2020.

[17] J. Nocedal and S. Wright, *Numerical Optimization*. Springer Science and Business Media, 2006.

[18] S. P. Bhat and D. S. Bernstein, "Finite-time stability of continuous autonomous systems," *SIAM Journal on Control and Optimization*, vol. 38, no. 3, pp. 751–766, 2000.

[19] B. Wie, *Space Vehicle Dynamics and Control*. American Institute of Aeronautics and Astronautics, 2008.